Electrochimica Acta 54 (2009) 1777–1783

Contents lists available at ScienceDirect

Electrochimica Acta

journal homepage: www.elsevier.com/locate/electacta

A study of iodine adlayers on polycrystalline gold electrodes by *in situ* electrochemical Rutherford backscattering (ECRBS)

Adrian Hightower[a,*,1], Bruce Koel[b], Thomas Felter[c]

[a] Department of Physics, Occidental College, 1600 Campus Road, Los Angeles, CA 90041, United States
[b] Department of Chemistry, Lehigh University, 6 E. Packer Ave., Bethlehem, PA 18015, United States
[c] Hydrogen and Metallurgy Sciences, Sandia National Laboratory, 7011 East Avenue, Livermore, CA 94550, United States

ARTICLE INFO

Article history:
Received 31 December 2007
Received in revised form 4 October 2008
Accepted 4 October 2008
Available online 1 November 2008

Keywords:
Polycrystalline gold electrode
Iodine adsorption
In situ RBS
Ion scattering
Gold
Etching

ABSTRACT

Iodine adsorption on a polycrystalline gold electrode was studied by *in situ* electrochemical Rutherford backscattering (ECRBS) using an ultrahigh vacuum (UHV)-electrochemical cell comprising of a thin-film silicon nitride window. The depth resolution of RBS allowed for measurement of nuclide concentration of the diffuse double-layer, electrode surface and near-surface regions. ECRBS measurements on the gold electrode, initially exposed to −500 mV vs. a platinum pseudo-reference electrode, in a potassium iodide solution, showed an increase in the 2.07 MeV iodine peak indicative of iodine adsorption. The surface concentration of the iodine adlayer was directly measured by ECRBS to be 1.3 ± 0.3 nmol/cm^2. ECRBS measurements on a gold electrode exposed to 1.5 V vs. a platinum pseudo-reference electrode, in a potassium iodide solution display a decrease in the 2.16 MeV gold peak and a shift to lower energies. Scanning electron microscopy images of electrodes studied by ECRBS displayed roughened surfaces consistent with gold dissolution. This work demonstrates the potential for *in situ* ECRBS using thin-film silicon nitride windows to become a powerful tool for the investigation of a wide range of electrochemical processes in areas such as corrosion, electrodeposition and electrocatalysis.

1. Introduction

The results of *in situ* electrochemical Rutherford backscattering (ECRBS) measurements of iodine adlayers on polycrystalline gold electrodes are reported in this work. Historically, it has been extremely challenging to design *in situ* spectroscopy experiments that directly measure the electrode composition under potentiodynamic control due to the liquid nature of the electrode environment. Such measurements are essential for correlating electrode performance to dynamic nanostructures at the electrode surface and the composition of the electrical double-layer. The advent of numerous *in situ* electrochemical diffraction and spectroscopy techniques has greatly expanded our understanding of the electrode–electrolyte interface (EEI). However, until recently the direct measurement of elemental surface composition could only be accomplished with techniques functioning in ultrahigh vacuum (UHV) environments [1–3]. This has limited direct elemental measurements of the EEI to a variety of *ex situ* experiments.

In contrast to other *in situ* electrochemical diffraction or spectroscopy techniques, ECRBS provides quantitative elemental analysis of the EEI. The *in situ* electrochemical techniques of Fourier transform infrared spectroscopy (ECFTIR) [4–6], scanning tunneling microscopy (ECSTM) [7–9], and surface X-ray diffraction (ECSXS) [10,11] provide information on bonding, topography, and crystalline phases at the EEI, respectively. As a complement to the aforementioned techniques, ECRBS is a rapid, non-destructive technique that measures the energy and intensity of backscattered ions whose energies are principally determined by the depth and the atomic number of the scattering center. Quantitative compositional analysis with an accuracy of up to 1% is enabled with RBS measurements by the fact that the number of scattered ions directly correlates to the number of scattering centers in the target [12]. When this technique is applied to a thin-film electrode deposited on a silicon nitride window separating the liquid and UHV environment, a compositional depth profile of the electrode and electrolyte can be obtained. ECRBS can probe large areas of the EEI under dynamic potential control. Currently, the analysis area for a given ECRBS measurement is ∼0.25 mm^2 and is primarily dictated by the area of the UHV window. The probe depth of the RBS ion beam allows observation of the EEI through a thin-film electrode window assembly (∼150 nm in thickness). The depth resolution of RBS (1–10 nm)

* Corresponding author. Tel.: +1 323 259 2826; fax: +1 323 341 4858.
E-mail address: hightower@oxy.edu (A. Hightower).
[1] SE member.

0013-4686/$ – see front matter © 2008 Elsevier Ltd. All rights reserved.
doi:10.1016/j.electacta.2008.10.027

[13] allows for measurement of nuclide concentration of the diffuse double-layer, surface and near-surface layers.

Ion beam techniques have been applied previously to investigate liquid–solid interfaces with reasonable success [14,15]. These *in situ* studies avoided the problem of sample corruption associated with transferring between liquid and vacuum environments. Morita et al. [16] studied lead desorption from SiO_2 with RBS using a liquid cell equipped with a 3-mm diameter, 5 μm thick Si window. In this case, a 9-MeV $^4He^{2+}$, 0.6-mm diameter beam at an ion flux of $1.9 \times 10^{13}/cm^2$ s was able to resolve Xe gas at atmospheric pressure as well as a 4-monolayer Pd thin film in separate experiments. This work was complicated by the use of a 5-μm thick Si window that significantly reduced the intensity and energy of the Pd peak. Penetrating this window necessitated the use of high-energy ion beams and leads to spectra complicated by increased inelastic scattering. More recently, Bouquillon et al. [17] used a liquid cell to perform PIXE analysis on lead-containing aqueous solutions. Pb at concentrations less than 10 ppm were resolved using a 3-MeV proton beam at ~1 nA through a 100 nm Si_3N_4 window. This work also identified bubble formation at regions of beam impact attributed to water radiolysis. It was determined that these bubbles could be eliminated with sufficient circulation of the solution. Lastly, RBS studies of the near surface region of aqueous sulfuric acid solutions and HCl-doped ice were carried out using analysis chambers employing differential pumping apertures [18].

ECRBS measurements were first demonstrated by Kötz et al. to study copper deposition on iridium and oxide formation on titanium [19]. This pioneering work utilized 3 MeV and 2.5 MeV $^4He^+$ beams through a 1.2-μm thick Si window along with iridium and titanium working electrodes, platinum counter electrodes and palladium pseudo electrodes. A number of challenges in ECRBS measurements were identified including the overlap of signals from low atomic number scattering centers situated closer to the beam source with signals from higher atomic number scattering centers situated further from the beam source. The loss of depth resolution due to peak broadening as scattered ions traversed the electrode and cell window was another challenge. It is important to note that the thickness of the window separating the electrochemical and vacuum environments plays a critical role on the impact of signal overlap and loss of depth resolution. Subsequent ECRBS studies have employed windows ranging in thickness from ~1 μm to study Cu, Ag and Pd deposition on Si [20] to 3.5 μm to study deuterium ingress into Zr–2.5 wt.% Nb [21]. The current study utilizes a much thinner 150-nm thick Si_3N_4 window in the hopes of minimizing the influences of signal overlap and the loss of depth resolution.

Adsorption of aqueous iodine on a polycrystalline gold electrode served as a benchmark in testing the current ECRBS system. The adsorption of ordered-monolayer phases of iodine on gold electrodes has been studied extensively by cyclic voltammetry [22–24], surface X-ray scattering (SXS) [25,26], STM [8,27–31], and electrochemical quartz crystal microbalance (ECQCM) [32,33] techniques. Iodine adlayers on single crystal gold surfaces demonstrate potential-dependent phase transitions [31,34] and are known to have a strong impact on the underpotential deposition of metal ions [30,35]. Iodide solutions are known to be an effective alternative to cyanide in both the chemical [36] and electrochemical [37] etching of gold. In these processes, electrons are removed from the metallic gold and the subsequent gold ions form strong complexes with iodide in solution.

$$Au^+_{(aq)} + 2I^-_{(aq)} \leftrightarrow AuI^-_{2(aq)} \quad (1)$$

Iodine and gold atoms provide scattering centers with large nuclear masses and thus, larger RBS signals as predicted by the formula for differential scattering cross-sections:

$$\frac{\partial\sigma}{\partial\Omega} = \left[\frac{Z_1 Z_2 e^2}{4E}\right]^2 \cdot \frac{4}{\sin^4\theta} \cdot \frac{\left[\sqrt{1-(A\sin\theta)^2} - \cos\theta\right]^2}{\sqrt{1-(A\sin\theta)^2}} \quad (2)$$

The differential scattering cross-section represents the probability of a scattering event with solid angle, Ω, to occur as a function of the atomic numbers of the incident and target ions, Z_1 and Z_2; the energy of the incident ion, E; the angle of incidence, θ; and the mass ratio of the incident ions to the target atoms, A. This work utilizes 2.3 MeV He^+ ions ($Z_1 = 4$) to investigate the adsorption of iodine ($Z_2 = 53$) and etching of gold ($Z_2 = 79$).

We seek to demonstrate the capabilities of ECRBS using a 150-nm thick Si_3N_4 window for elemental characterization of electrochemical interfaces by measuring iodine adsorption on a polycrystalline gold electrode as well as etching of a gold electrode.

2. Experimental

Fig. 1a displays a sealed, UHV-electrochemical cell with a 1.5-mL liquid-filled-well that was fabricated from a vacuum-grade epoxy resin (Torr Seal®) and a 0.25-mm^2, 150-nm thick Si_3N_4 window. This UHV-electrochemical cell was placed directly inside the RBS

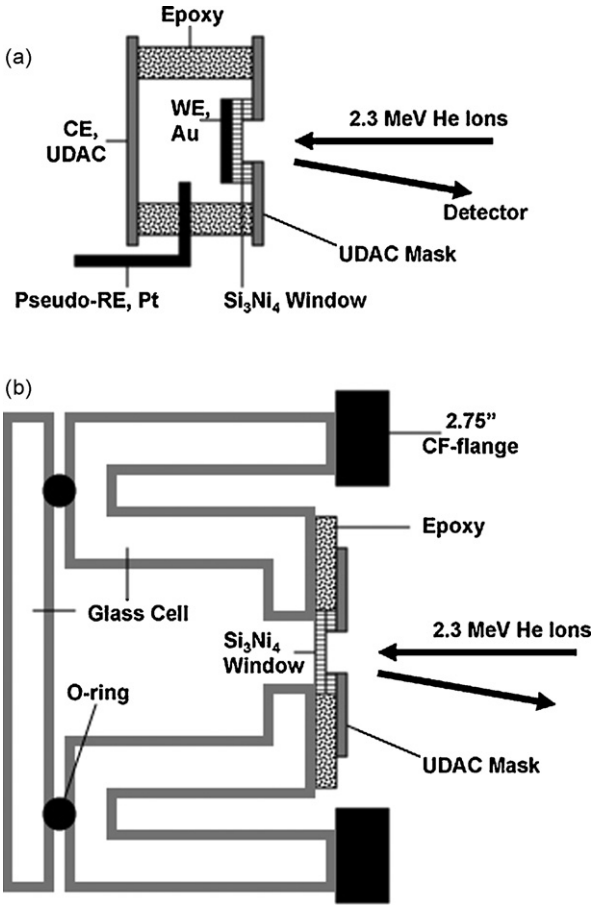

Fig. 1. (a) Schematic drawing of the UHV-electrochemical cell used in the ECRBS study of Au dissolution and I adsorption on a polycrystalline Au electrode. The cell incorporates a 0.25-mm^2 UDAC mask; a 0.25-mm^2, 150-nm thick Si_3N_4 window; a 10-nm thick Au working electrode (WE), a 125-μm diameter Pt wire to act as a pseudo-reference electrode (RE), a UDAC counter electrode (CE), and a sealed 1.5-mL liquid well. (b) Schematic drawing of the UHV-liquid cell used to test window stability. The cell incorporates a 0.25-mm^2 UDAC mask with a 0.25-mm^2, 500-nm thick Si_3N_4 window.

vacuum chamber (base pressure of 2×10^{-8} Torr). A second UHV-liquid cell (Fig. 1b) used a 500-nm thick Si_3N_4 window and a 2.75" Conflat® flange with a Pyrex®–stainless steel seal to interface the RBS UHV chamber with an external electrochemical cell at ambient pressure and temperature. The first UHV-electrochemical cell was utilized to study iodine on gold electrodes, while the UHV-liquid cell was used to test the stability of the Si_3N_4 window separating the UHV environment from a two molar potassium iodide solution and xenon gas.

A working electrode was formed by sputtering a 10-nm gold film onto a Si_3N_4 window (SPI Supplies). The Si_3N_4 window, mounted on a 200-μm thick Si frame, was rated to withstand a pressure differential of 1 atm. A 125-μm diameter Pt wire was used as a pseudo-reference electrode and an ultradense amorphous carbon (UDAC) substrate served as the counter electrode. The three-electrode UHV-electrochemical cell was interfaced to an ACM Gill AC potentiostat via coaxial UHV feedthroughs. Prior to ECRBS runs, electrochemical measurements were performed on the polycrystalline gold electrodes in UHV-electrochemical cells placed directly into the RBS UHV chamber. Cyclic voltammograms with scan rates of 100 mV/min in 0.5 H_2SO_4 + 0.1 mM KI solutions were used to characterize the quality of the electrochemical environment when the UHV-electrochemical cell was placed into the UHV chamber at pressures of 8×10^{-8} Torr. In order to simplify the RBS spectra, an electrolyte of 7 mM KI prepared from 18 MΩ cm water (B&J Brand) and analytical grade reagents (Alpha Aesar, 99.99% KI) was used for the ECRBS studies. A low concentration potassium iodide solution was chosen in the hopes of measuring iodide concentration in an extended diffuse layer as a function of distance from the electrode.

A 2.3-MeV He^+ ion beam at a current of 40 nA and a spot size of 0.4 mm^2 was aligned through a 0.2-mm^2 UDAC aperture before striking the 0.25 mm^2 Si_3N_4 window. The UDAC aperture served to mask the Si frame housing the Si_3N_4 window, thereby reducing its contribution to the RBS spectra. The RBS spectra were acquired using an Ortec Ion-Implanted-Silicon Charged-Particle detector set at $\theta = 164^\circ$ relative to the incident ion beam. Spectra were obtained over 1024 channels with a resolution of <20 keV. RBS spectra were normalized to the total number of detected ions. The accelerator and beam lines were protected from possible window failure by a VAT Series 75, fast-closing valve system.

Measured spectra were compared to simulations produced by the Rutherford Universal Manipulation Program (RUMP) code [38]. Electrodes were held at a given, constant potential while a RBS measurement was performed. The average measurement time used to obtain a RBS spectrum was about 10 min. Finally, a Cambridge 360 Scanning Electron Microscope (SEM) was used to characterize the sputtered gold electrodes before and after ECRBS gold etching studies.

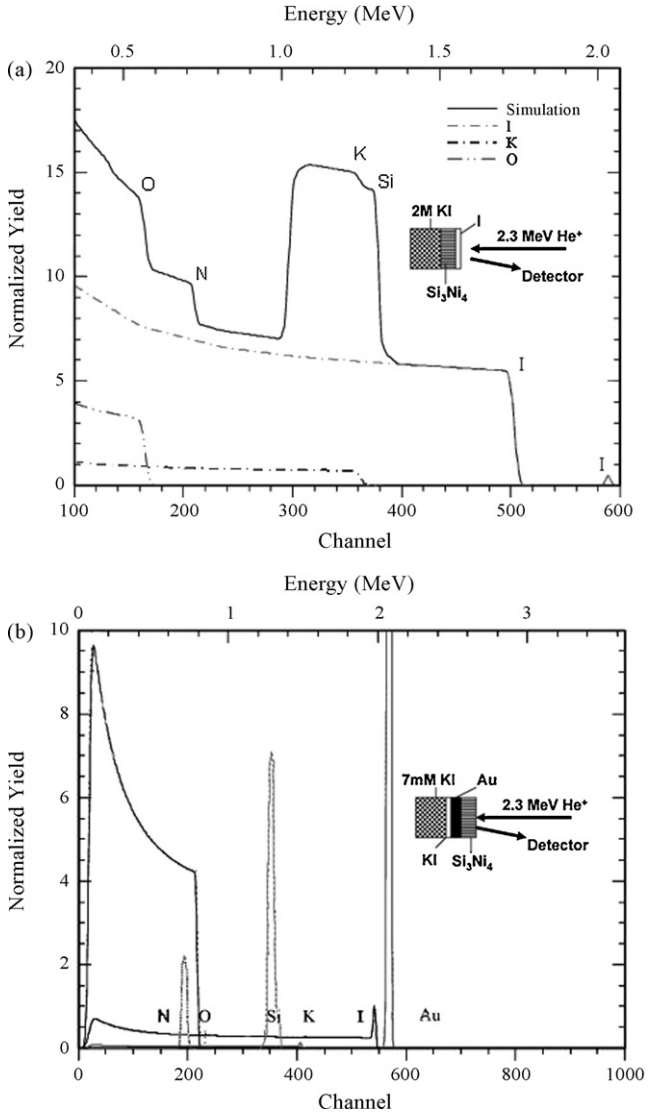

Fig. 2. (a) RUMP simulation of the RBS spectra from a 2.3-MeV He^+ beam incident on a 0.2-nm iodine film, 900-nm Si_3N_4 window, followed by a 50-μm 2 M KI aqueous solution. The iodine monolayer peak at 2.05 MeV can be distinguished from the iodine in the solution that follows the Si_3N_4 window. The thick Si_3N_4 window results in the oxygen, potassium, and iodine solution signals are shifted to lower energy. (b) RUMP simulation of the RBS spectra from a 2.3-MeV He^+ beam incident on a thin Si_3N_4 window, followed by an 8-nm Au film, followed by a single adlayer of KI, followed by a 7 mM KI aqueous solution. The iodine adlayer peak at 2 MeV can be distinguished from the iodine in the solution. The gold peak is much larger than the iodine peak primarily because the Au film is relatively thick.

3. Results

3.1. Simulations

Several RUMP simulations were performed in order to determine the viability of the ECRBS technique. A variety of Si_3N_4 window and gold electrode thicknesses were simulated to deter-

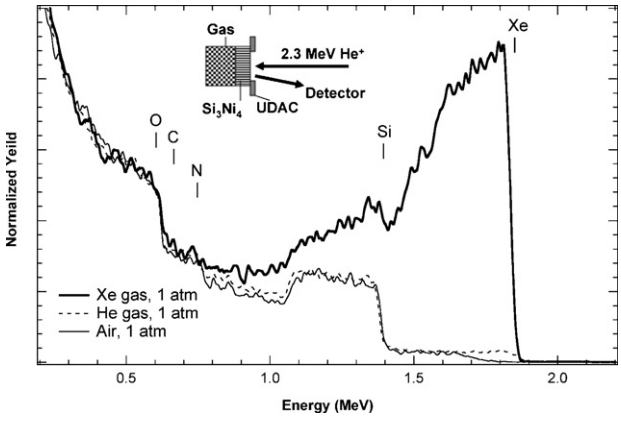

Fig. 3. RBS spectra of xenon, helium, and air through a 500-nm Si_3N_4 window. The 1.85 MeV xenon edge is observed with significant modification from a normal RBS plateau shape due to the low density of the gas and hence deep penetration of the ions. The UDAC mask blocks deeply scattered ions from reaching the detector. The widths of the Si and N peaks are consistent with a nominal 500-nm thick Si_3N_4 window. The Xe and O features are shifted to lower energies due to slowing of the incident ions by the 500-nm Si_3N_4 window.

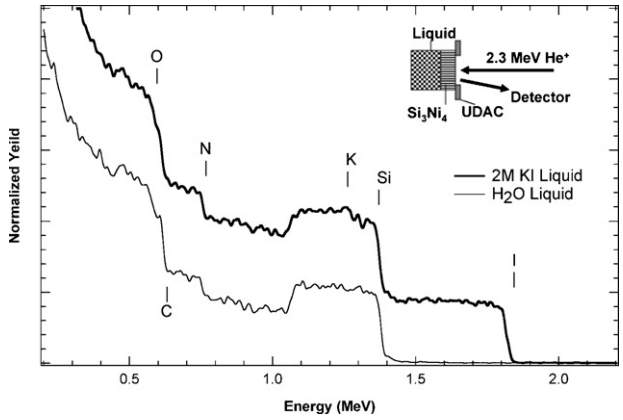

Fig. 4. RBS spectra of a 2-M KI aqueous solution through a 500-nm Si_3N_4 window. The iodine plateau at 1.85 MeV can be observed along with a potassium plateau at 1.25 MeV. The widths of the Si and N peaks are consistent with a nominal 500-nm thick Si_3N_4 window. The I, K and O plateaus are shifted to lower energies due to slowing of the incident He^+ ions by the 500-nm Si_3N_4 window.

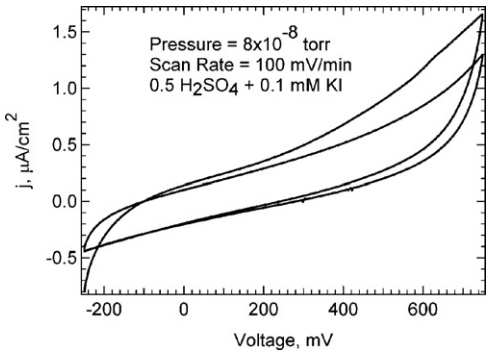

Fig. 5. A cyclic voltammogram of a polycrystalline Au electrode in an UHV-electrochemical cell using 0.5 M H_2SO_4 + 1 mM KI, scanned at 100 mV/min vs. a Pt pseudo-reference electrode that was performed with the UHV-electrochemical cell in the RBS chamber at a pressure of 8×10^{-8} Torr.

mine their impact on ECRBS spectra. Simulations yielded the expected phenomenon of a decrease in onset energy from scattering centers that followed the Si_3N_4 window in the ion beam path. This decrease in energy (slowing) of the ions is a result of the stopping power associated with traversing the window. This stopping power results primarily from electronic excitation of the window material and is a function of the energy and mass of the incident particles and the composition of the window. Ions can also lose energy as they traverse the gold electrode and the electrolyte as well as after their back scattering collision during their path to the detector.

Evidence of this decrease in onset energy is observed in Fig. 2a which displays a RUMP simulation of an RBS spectra from a 2.3-MeV He^+ beam incident on an 0.2-nm iodine film, followed by a 900-nm Si_3N_4 window, followed by a 50-μm 2 M KI aqueous solution. The iodine onset at 1.7 MeV from the 2 M KI solution is shifted to lower energy relative to the 2.04 MeV peak of the unobstructed 0.2-nm iodine film. In addition, the oxygen plateau at 0.58 MeV of the solution is shifted to energies below the nitrogen plateau at 0.73 MeV despite oxygen's higher atomic number.

Conclusions were drawn from comparisons of ECRBS data to simulated spectra from estimated concentrations and distributions of key elements: Si, N, Au, and I. A RUMP simulation of a 2.3-MeV He^+ beam incident on a 150-nm Si_3N_4 window, followed by an 8-nm thick gold thin film, followed by a 0.2-nm KI adlayer, followed by a 80-μm 7 mM KI aqueous solution is shown in Fig. 2b. The potassium iodide adlayer peak at 2 MeV can be distinguished from the aqueous iodine background as well as the gold film. The proximity of the iodine and gold peaks suggest that roughness in the gold electrode could cause overlap between the peaks. The 2 MeV iodine peak of the KI film is shifted to lower energies relative to the 2.04 MeV peak of the unobstructed iodine film displayed in Fig. 2a.

3.2. Liquid and gas studies

The viability of the Si_3N_4 window to successfully isolate the UHV and liquid environments was tested with the UHV-liquid cell, which allows for easy changing of various gases and liquids such as saturated potassium iodide solutions and xenon gas. In particular, the durability of the epoxy seals at the interfaces of glass, silicon, and electrode leads were tested. The seals were found to last reliably for the length of the experiments (~4 h) provided that the epoxy was allowed to cure for the recommended time.

RBS spectra of xenon, helium, and air through a 500-nm Si_3N_4 window are shown in Fig. 3. The xenon edge at 1.85 MeV can be observed with a significant change from the usual plateau shape found in condensed matter samples. The change in shape is due to the UDAC mask blocking deeply scattered ions from reaching the detector. The low density of gas compared to condensed matter results in scattering events occurring deep in the sample, millimeters below the mask. For example, 2 MeV He ions travel a millimeter before loosing 0.3 MeV of energy. From this depth, the UDAC mask blocks the line of sight path to the detector. The silicon edge at 1.40 MeV in Fig. 3 is made up of backscattered ions from the 500-nm Si_3N_4 window as well as the 200-μm Si frame. The width of the silicon plateau is defined by and consistent with a nominal 500-nm thick Si_3N_4 window. The silicon signal from the 200-μm Si frame extends to lower energies than the plateau and contributes to the background of lower energy signals. The xenon and oxygen features are shifted to lower energies due to the slowing of the incident He^+ ions by the 500-nm Si_3N_4 window. The carbon feature is primarily a result of backscattering from the UDAC mask and experiences no such shift.

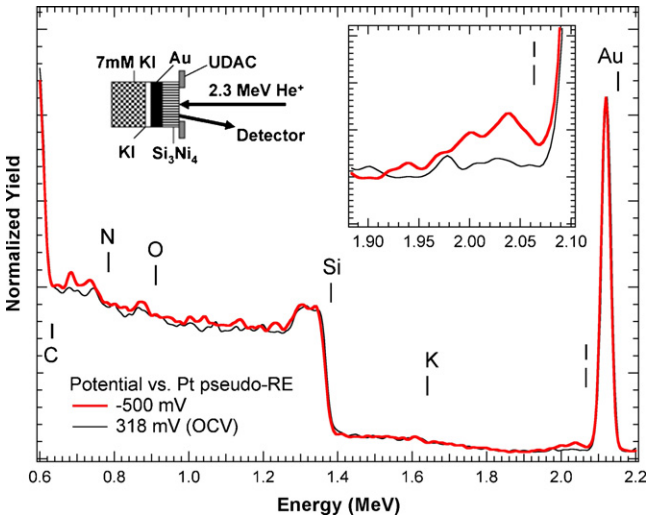

Fig. 6. ECRBS spectra of a polycrystalline Au electrode in 7 mM KI held at the open circuit voltage of 318 mV and −500 mV vs. a Pt pseudo-reference electrode. The initial application of a negative potential results in an increase in the iodine peak, 2.07 MeV, indicative of iodine adsorption, as shown more clearly in the inset. The widths of the Si and N peaks are consistent with a nominal 150-nm thick Si_3N_4 window.

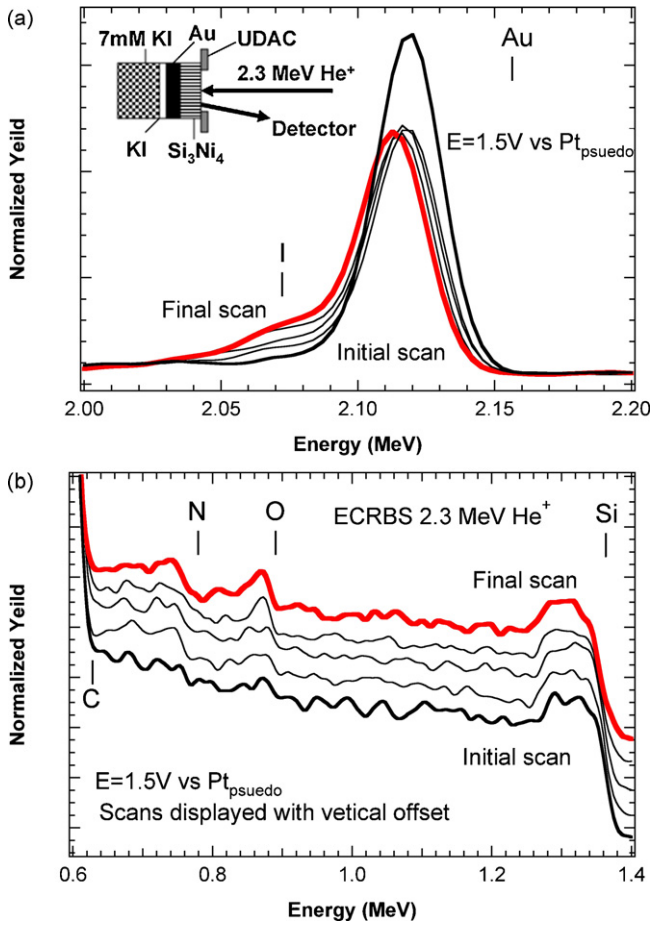

Fig. 7. RBS spectra of the oxidation of an Au electrode held at a potential of 1.5 V vs. a Pt pseudo-reference electrode. The top panel (a) shows decrease of the gold peak, 2.12 MeV, indicative of roughening and gold dissolution. The bottom panel (b) shows an increase and sharpening of the oxygen peak at 0.87 MeV.

Fig. 4 displays RBS spectra from a 2-M KI aqueous solution obtained through a 500-nm Si_3N_4 window. The iodine plateau at 1.85 MeV can be observed along with a potassium plateau at 1.25 MeV. The silicon plateau at 1.40 MeV is consistent with a nominal 500-nm thick Si_3N_4 window supported by a 200-μm Si frame and is comparable to the silicon in Fig. 3. The intensity of the iodine feature indicates no significant iodine adsorption on the Si_3N_4 window. The height of the iodine feature relative to the silicon feature is comparable to the heights simulated in Fig. 2a. These intensities are complicated by the contribution of the Si frame to the silicon edge. The iodine, potassium, and oxygen features are shifted to lower energies due to slowing of the incident He^+ ions by the 500-nm Si_3N_4 window. Again the carbon feature is primarily a result of backscattering from the UDAC mask and experiences no such shift.

3.3. Electrochemical performance and ion beam measurements

The capability of the UHV-electrochemical cell inside the RBS UHV chamber at a pressure of 8×10^{-8} Torr was tested prior to ECRBS tests. Fig. 5 displays a cyclic voltammogram of a polycrystalline gold electrode on a 500-nm thick Si_3N_4 window obtained in a solution of 0.5 H_2SO_4 + 1 mM KI, and scanned at 100 mV/min vs. a Pt pseudo-reference electrode. The voltammogram demonstrates that potentiodynamic control was possible using UHV-electrochemical cell, but only with limited analytical capability. The poor resolution of the CV scan indicates a non-ideal electrochemical environment that is likely associated with a fouled electrode surface.

Fig. 6 displays ECRBS spectra of a 10-nm thick polycrystalline gold electrode in 7 mM KI solution obtained at open circuit and held at a small negative potential of −0.5 V. The spectra show distinct peaks for gold and adsorbed iodine with onset edges at 2.16 and 2.07 MeV, respectively. Plateaus that are approximately 0.1 MeV wide can be observed at 1.40 and 0.75 MeV for the silicon and nitrogen components respectively, due to the Si_3N_4 window. The onset energy of these silicon and nitrogen plateaus correspond to those observed in Figs. 3 and 4, while the width (0.1 MeV) corresponds to the nominal 150-nm thickness of the Si_3N_4 window. Ions backscattered from the 200-μm thick Si-window substrate and the UDAC mask produce signals below 1.40 and 0.6 MeV, respectively. The undesirable silicon background signal (0–1.40 MeV) indicates a slight misalignment of the UDAC mask, He^+ ion beam, and silicon frame. Minor peaks from potassium and oxygen can be observed at 1.63 and 0.91 MeV, respectively.

In order to observe dissolution of the gold electrode, the cell was driven to anodic potentials of 1.5 V. Several RBS spectra of the gold electrode, obtained sequentially at about 10 min/spectra. Fig. 7a shows an initial reduction in area and broadening of the 2.16 MeV gold peak to lower energies. Fig. 7b shows the silicon, oxygen, nitrogen and carbon onset regions (0.62 MeV) in greater detail. The unwanted Si background (0–1.4 MeV) arises from the 200-μm thick Si-window frame. Since the backscattered yield depends on Z^2, where Z is the atomic number, light elements are easily obscured

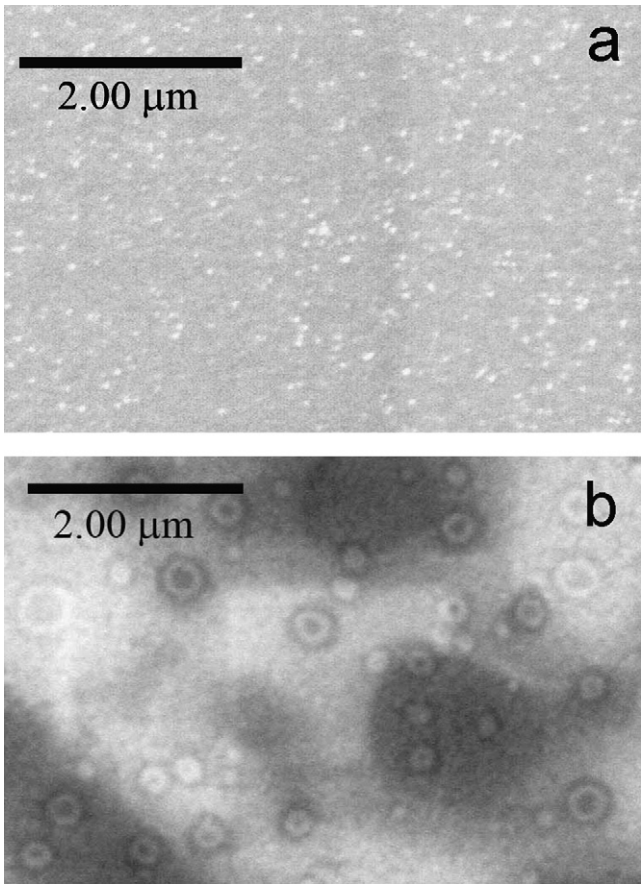

Fig. 8. SEM images of the10-nm thick sputtered Au film before (a) and after ECRBS Au dissolution experiment (b). The Au film is initially fairly homogeneous, but after the dissolution experiments, shows altered Au regions with a diameter of ~300 nm that arise from radiolysis and/or Au dissolution.

by the presence of the Si background. More accurate mask alignment should reduce this significantly, making it easier to detect and quantify the concentration of light elements, such as oxygen.

3.4. Electrode morphology

Fig. 8 displays SEM images of the initial 10 nm-thick sputtered gold electrode and the electrode after the ECRBS study. The electrode was initially fairly homogeneous (Fig. 8a), but the electrode surface appeared roughened and contained altered regions of ~300 nm in size after the ECRBS experiments (Fig. 8b). Subsequent energy dispersive X-ray (EDX) spectroscopy measurements could not detect iodine at the electrode surface.

4. Discussion

RUMP simulations suggested that ECRBS would have the capability to directly measure adsorbed iodine species as a function of gold electrode potential. Additionally, RUMP simulations predicted ECRBS would have the capability of measuring gold etching rate as a function of gold electrode potential. A dilute salt solution was employed in the hopes of measuring iodide concentration in an extended diffuse layer as a function of distance from the electrode. Initial ECRBS experiments reported in this paper display the aforementioned capability but with limited resolution.

An increase in iodine concentration at the electrode surface, as indicated by the increase in area under the iodine peak in the RBS spectra, was observed when a negative potential of −500 mV vs. a Pt pseudo-reference electrode was applied. There was a relatively small amount of adsorbed iodine initially despite electrode exposure to the solution for 15 min prior to the ECRBS measurement. Iodine monolayers are known to form spontaneously on clean gold electrodes within minutes of exposure. The slow adsorption kinetics of iodide on the studied gold electrode can be attributed to the presence of contaminants on the electrode surface. Once a potential was applied to the electrode, an iodine monolayer formed within the time required for one ECRBS measurement (~10 min). It is not obvious that the application of a negative potential should attract iodide to the electrode surface. However, an increase in active surface sites as a result of the reduction of contaminant surface oxides could explain the formation of an iodine monolayer with the applied negative potential.

The determination of the amount of surface iodine is complicated by the UHV-electrochemical cell construction. The size of the mask opening, and therefore the amount of the incident beam that actually hits the electrode, is not precisely known. However, by comparing the measured areas of the iodine and gold peaks to RUMP simulations and assuming an initially smooth, 10-nm thick gold electrode, we can make an estimate of the amount of iodine in the adlayer. An iodine surface concentration of 1.3 ± 0.3 nmol/cm^2 was measured for the iodine adlayer, which is close to the monolayer value of 1.04 nmol/cm^2 reported by Rodriguez et al. [39]. This constitutes reasonable agreement considering the large uncertainty in the thickness and roughness of the polycrystalline gold electrode used in the ECRBS experiment.

The use of a Pt wire as a pseudo-reference electrode complicated the determination of the onset potentials for gold dissolution from the polycrystalline electrode. The application of 1.5 V was accompanied by a large initial dissolution of gold, as indicated by the decrease in area of the 2.16 MeV Au peak. Further measurement showed a redistribution of the Au peak to lower energies with only minor changes in peak area. The initial rapid dissolution of gold is attributed to electrochemical etching that removed 28% of the gold thin film within 10 min. This corresponds to an etching rate of 0.28 nm/min. This value is low compared to typical chemical gold etching processes (~10 μm/min). Although a potential of 1.5 V was applied to the system, the etching solution was limited by a dilute salt concentration (7 mM KI) and the absence of a proper electrolyte or buffer. It is also likely that the application of 1.5 V resulted in the formation of gold oxide at the EEI. The presence of gold oxide would significantly decrease the kinetics of gold dissolution, reduce the value for the etching rate, and explain why subsequent measurements at 1.5 V did not result in significant dissolution of gold. The presence of gold oxide may contribute to the slight increase and sharpening of the 0.87 MeV oxygen peak, though it is difficult to draw definitive conclusions from the lower energy edges. The increased overlap among the 2.07 MeV iodine and 2.16 MeV gold peaks is likely because of the roughening of the oxidized electrode and formation of gold–iodide complexes. These observations are consistent with the results of previous chronocoulometry studies of iodine adsorption on gold electrodes [22] and ECSTM studies at 1.3 V on the oxidation of gold electrodes [40].

The ECRBS studies were carried out over the course of 1 h with 1.5 mL of stagnant electrolyte. The system as configured here is susceptible to radiolysis and the formation of bubbles near the electrode surface would complicate interpretation of the RBS spectra. Nevertheless, we can clearly observe the concomitant formation of an iodine layer and dissolution of the gold electrode. Improvements in the technique in later experiments should include addition of a standard reference electrode, incorporation of a mechanism for electrolyte circulation, and better electrochemical characterization.

The depth resolution of ECRBS (1–10 nm) as reported here is relevant for measuring aspects of diffusion in the EEI and phase transitions in electrode materials as a function of potential, but provides limited information regarding adsorbed monolayers at the electrode surface and concentrations of adspecies in the Stern layer. Channeling and blocking experiments in ECRBS utilizing single-crystal electrode/window assemblies may be one approach to increasing this capability. Medium energy ion scattering (MEIS) employs lower energy ion beams (~100 keV) and can have much better depth resolution (0.5–1 nm) than RBS techniques. However, the use of MEIS in such an electrochemical approach (ECMEIS) may require even thinner windows than employed in this work. The challenge will be to design an electrochemical cell with such windows that can isolate the corresponding UHV and liquid environments. Thus, while ECRBS is useful for the elemental characterization of bulk electrodes, ECMEIS may be a better approach for quantitative elemental analysis of electrode surface species. To our knowledge, no such ECMEIS experiment has been made previously.

5. Conclusions

The demonstrated *in situ* ECRBS system using a 150-nm silicon nitride window provides a new *in situ* elemental analysis technique for investigating electrochemical processes at the electrode–electrolyte interface (EEI) under potential control. Iodine accumulation of 1.3 ± 0.3 nmol/cm^2 at a polycrystalline gold electrode under a negative potential was directly measured by ECRBS. The formation of an iodide layer and dissolution of the gold electrode was also directly observed by ECRBS. We have suggested changes that will improve the technique, and we point out that a similar approach utilizing channeling and blocking in RBS or application of MEIS should enable characterization of electrode adlayers and concentration in the Stern layer with submonolayer resolution. We believe that ECRBS can further the understanding of a wide range of electrochemical processes, in particular corrosion, elec-

trodeposition, and electrocatalysis by enabling new investigations of the kinetics of nuclide adsorption and desorption.

Acknowledgements

The authors thank Merck & Co., Inc. and the United Negro College Fund for their financial support through a postdoctoral research fellowship. The authors express their deep appreciation to Florian Mansfeld of the University of Southern California and the journal referees for their guidance. Work at Lawrence Livermore National Laboratory was performed under the auspices of the U.S. Department of Energy by the University of California, Lawrence Livermore National Laboratory under Contract No. W-7405-Eng-48.

References

[1] G.A. Somorja, Introduction to Surface Chemistry and Catalysis, Wiley-Interscience, New York, 1994.
[2] A.T. Hubbard, Chemical Reviews 88 (4) (1988) 633.
[3] M.P. Soriaga, Progress in Surface Science 39 (4) (1992) 325.
[4] T. Iwasita, F.C. Nart, Progress in Surface Science 55 (4) (1997) 271.
[5] T. Iwasita, Journal of the Brazilian Chemical Society 13 (4) (2002) 401.
[6] X.F. Lin, B. Ren, Z.Q. Tian, Journal of Physical Chemistry B 108 (3) (2004) 981.
[7] L. Piccolo, et al., Surface Science 566 (2004) 995.
[8] K. Itaya, Progress in Surface Science 58 (3) (1998) 121.
[9] R. McHardy, W.H. Haiss, R.J. Nichols, Physical Chemistry Chemical Physics 2 (7) (2000) 1439.
[10] M.G. Samant, et al., Journal of Physical Chemistry 92 (1) (1988) 220.
[11] V.R. Stamenkovic, et al., Journal of the American Chemical Society 125 (9) (2003) 2736.
[12] C. Jeynes, et al., Surface and Interface Analysis 25 (4) (1997) 254.
[13] H. Paul, D. Semrad, A. Seilinger, Nuclear Instruments & Methods in Physics Research Section B-Beam Interactions with Materials and Atoms 61 (3) (1991) 261.
[14] C.E. Vallet, et al., Journal of the Electrochemical Society 144 (4) (1997) 1289.
[15] K. Padmanabhan, Surface and interface analysis 10 (2–3) (1987) 126.
[16] K. Morita, et al., Radiation Physics and Chemistry 49 (6) (1997) 603.
[17] A. Bouquillon, et al., Nuclear Instruments & Methods in Physics Research Section B-Beam Interactions with Materials and Atoms 188 (2002) 156.
[18] U.K. Krieger, et al., Science 295 (5557) (2002) 1048.
[19] R. Kötz, et al., Electrochimica Acta 31 (2) (1986) 169.
[20] J.S. Forster, et al., Nuclear Instruments & Methods in Physics Research Section B-Beam Interactions with Materials and Atoms 28 (3) (1987) 385.
[21] J.S. Forster, et al., Nuclear Instruments & Methods in Physics Research Section B-Beam Interactions with Materials and Atoms 56–7 (1991) 821.
[22] A.C. Chen, et al., Journal of Electroanalytical Chemistry 467 (1–2) (1999) 342.
[23] A. Hamelin, Journal of Electroanalytical Chemistry 142 (1–2) (1982) 299.
[24] J.P. Bellier, A. Hamelin, Comptes Rendus Hebdomadaires Des Seances De L Academie Des Sciences Serie C 280 (25) (1975) 1489.
[25] J. Wang, et al., Physical Review B 46 (16) (1992) 10321.
[26] B.M. Ocko, G.M. Watson, J. Wang, Journal of Physical Chemistry 98 (3) (1994) 897.
[27] X.P. Gao, et al., Journal of Physical Chemistry 98 (33) (1994) 8086.
[28] K. Itaya, et al., In situ scanning tunneling microscopy of organic molecules adsorbed on iodine-modified Au(1 1 1), Ag(1 1 1), and Pt(1 1 1) electrodes, in Solid–Liquid Electrochemical Interfaces (656) (1997) 171.
[29] N.J. Tao, S.M. Lindsay, Journal of Physical Chemistry 96 (13) (1992) 5213.
[30] T. Yamada, N. Batina, K. Itaya, Surface Science 335 (1–3) (1995) 204.
[31] T. Yamada, N. Batina, K. Itaya, Journal of Physical Chemistry 99 (21) (1995) 8817.
[32] N.Y. Gu, L. Niu, S.J. Dong, Electrochemistry Communications 2 (1) (2000) 48.
[33] H.W. Lei, H. Uchida, M. Watanabe, Langmuir 13 (13) (1997) 3523.
[34] N. Batina, T. Yamada, K. Itaya, Langmuir 11 (11) (1995) 4568.
[35] K. Ogaki, K. Itaya, Electrochimica Acta 40 (10) (1995) 1249.
[36] W. Eidelloth, R.L. Sandstrom, Applied Physics Letters 59 (13) (1991) 1632.
[37] Z. Hu, T. Ritzdorf, Journal of the Electrochemical Society 154 (10) (2007) D543.
[38] Y. Kido, Nuclear instruments & methods in physics research., Section B, Beam interactions with materials and atoms 9 (3) (1985) 291.
[39] J.F. Rodriguez, T. Mebrahtu, M.P. Soriaga, Journal of Electroanalytical Chemistry 233 (1–2) (1987) 283.
[40] M.A. Schneeweiss, D.M. Kolb, Solid State Ionics 94 (1–4) (1997) 171.